Research Article: Open Access

VIBGYOR ePress

International Journal of Nanoparticles and Nanotechnology

ISSN: 2631-5084

The Photoluminescent and Magnetic Properties of Mn^{2+} Ions at the Interface of Core/Shell Mn-Doped Nanocrystals

Boping Yang*

Yancheng Institute of Technology, China

Abstract

The properties of Mn-doped Nanocrystals (NCs) with increasing binding symmetry and ZnSe:Mn/ZnSe NCs under different temperatures were investigated to demonstrate the relation between the strength of crystal field and covalency. The position of Mn ions in NCs were accurately controlled at the interface of the core/shell Mn-doped NCs. Transmission Electron Microscopy (TEM) images and X-ray Diffraction (XRD) spectra were used to demonstrate the structure of the NCs. Magnetic properties of the NCs were gained through the Electron Paramagnetic Resonance (EPR) spectra. Photo Luminescent (PL) properties reflect the strength of crystal filed in Mn-doped NCs and the magnetic properties demonstrate the change of covalency. The relationship between the crystal field and covalency was indicated by structure-dependent and temperature-dependent properties of Mn-doped NCs.

Keywords

Mn-doped nanocrystals, Crystal field, Covalency

Introduction

Nanocrystals (NCs) have been wildly studied due to the properties different from bulk materials [1-3]. Researchers focus on doped NCs for some excellent performances compared with un-doped NCs [4-8]. As one kind of doped NCs, Mn-doped NCs have gain great attention due to their Photo Luminescent (PL) properties and been used for devices manufacturing [9,10]. Further, Mn-doped NCs also show some magnetic properties which were detected by Electron Paramagnetic Resonance (EPR) spectra [9,11,12].

It is well known that the emission of Mn^{2+} in NCs is attributed to the $^4T_1$ to $^6A_1$ transition [7,13,14]. This emission has been found to be effected by shell thickness in core/shell ZnSe and CdS/ZnS NCs [15-17]. The change of luminescent color was suggested to be resulted from change of the splitting of the $^6A_1$ state of Mn^{2+} ions due to different shell thickness. Additionally, enhanced crystal field was demonstrated to be the reason for bigger splitting of the $^6A_1$ state [18], which illustrated that stronger crystal field, resulted in PL red-shift.

Due to unpaired electrons, the local environment of Mn^{2+} ions in Mn-doped NCs has been explored by EPR spectra [9,11,12,13]. The values of superfine splitting constant (A) of EPR spectra can evidence the position of Mn^{2+} ions [12,19,20]. Additionally, the EPR spectra also demonstrate the covalency between the anion and cation [8,21]. Larger value of A suggested weaker covalency [12,20,21]. In Mn-CdSe NCs, larger A value was suggested to be resulted from the Mn aggregation at the surface of the NC, which implied reduced covalency [14]. Similar report was shown in core/shell CdS/ZnS NCs [22].

Our previous work has investigated the relationship between crystal filed and covalency by Mn-doped NCs with different binding symmetry [8]. To a certain degree, this structure-dependent result clarified the relationship

***Corresponding author:** *Boping Yang, Yancheng Institute of Technology, Yancheng 224051, P. R. China, Tel: 86-0515-88168187, E-mail: bpyang023@163.com*

Received: March 26, 2017: **Accepted:** July 10, 2017: **Published:** July 12, 2017

Citation: Yang B (2017) The Photoluminescent and Magnetic Properties of Mn^{2+} Ions at the Interface of Core/Shell Mn-Doped Nanocrystals. Int J Nanoparticles Nanotech 3:009

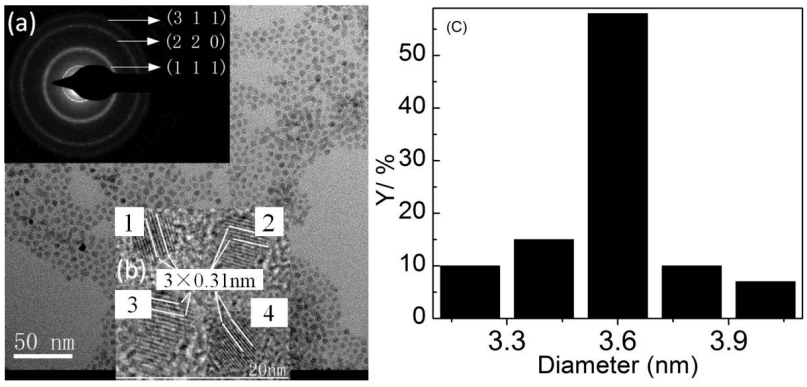

Figure 1: TEM image of ZnSe:Mn/ZnSe NCs at room temperature. Insert (a), (b) and (c) are the electron diffraction pattern, HRTEM image (1, 2, 3, 4 are single crystal at different area) and size distribution, respectively.

mentioned above. In this work, both the structure-dependent and temperature-dependent properties of Mn-doped NCs were considered for further understanding of this relationship.

Experimental Details

All Mn-doped NCs in this work were synthesized through the method as shown in our previous work [8]. The process includes core fabrication, elimination of residual Mn^{2+} in the solution and shell growing. The synthesis procedure in this work contained the elimination of the residual Mn in the solution, which suggested there were no Mn^{2+} ions in the ZnS shell. The synthesis process are as follows: (1) ZnSe cores preparation and purification; (2) Mn adsorption on ZnSe at 120 °C and the elimination of the residual Mn in the solution; (3) ZnSe shell growth at 270 °C. This could demonstrated that the Mn^{2+} ions were at the interface of the core/shell NCs and no Mn^{2+} ions were at the surface. Furthermore, EPR spectra also suggest that the Mn^{2+} ions were at the interface of core and shell of the NCs. The NCs are ZnSe:Mn/ZnS (sample I), ZnSe/ZnS(1ML):Mn/ZnS (sample II), ZnSe/ZnS(2ML):Mn/ZnS (sample II) and ZnSe:Mn/ZnSe (sample IV), respectively. Location of Mn^{2+} ions at the interface of the core/shell NCs results in increasing binding symmetry from sample I to IV [8]. Transmission Electron Microscopy (TEM) images were gained from a Tecnai G2 Transmission Electron Microscope (FEI). X-ray Diffraction (XRD) spectra were recorded on a D/max 2500VL/PC diffractometer using Cu Kα radiation. PL spectra were gained on a FLS920 F900 luminescence spectrometer (Edinburgh). EPR spectra were measured with an X-band EMX-10/12 spectrometer (Bruker). ZnSe:Mn/ZnSe NCs were spin coated on quartz glass and mounted in a vacuum liquid nitrogen cryostat for the temperature-dependent measurement. The temperature range was from 77 to 297 K.

Results and Discussion

Figure 1 and the inserts show the typical TEM images, the selective area electron diffraction pattern (SAEDP, insert (a)), and high-resolution TEM (HRTEM) images of single crystal at different areas (insert (b)). The ZnSe:Mn/ZnSe NCs are with cubic zinc blende structure, which is demonstrated by the SAEDP. The rings corresponding to (1 1 1), (2 2 0), and (3 1 1) diffraction can be observed clearly in insert (a) of Figure 1. The HRTEM images indicate that there is no lattice distortion after the Mn adsorption and shell coating. Histogram (c) in Figure 1 shows that the NCs are at good size distribution. The other three NCs samples show similar results.

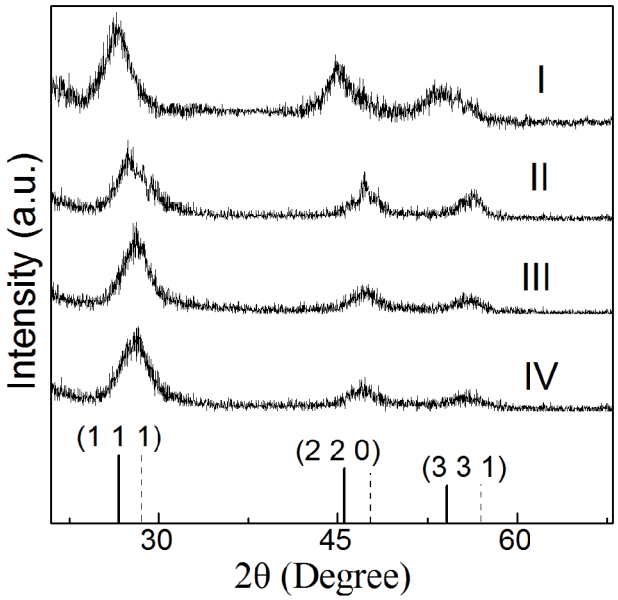

Figure 2: X-ray diffraction patterns for all samples. The XRD patterns corresponding to bulk cubic ZnSe (solid) and ZnS (short dot) are shown at the bottom.

The XRD spectra of the four samples are shown in Figure 2. The XRD patterns indicate that all samples are zinc blende phase, according with the results of SAEDP in Figure 1. No Mn diffraction peaks are observed in all the samples, which indicate that Mn^{2+} ions had doped

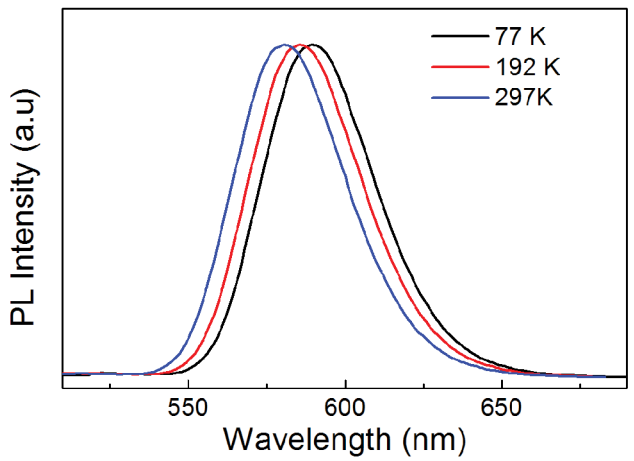

Figure 3: Typical PL spectra of the ZnSe:Mn/ZnSe NCs under different temperature.

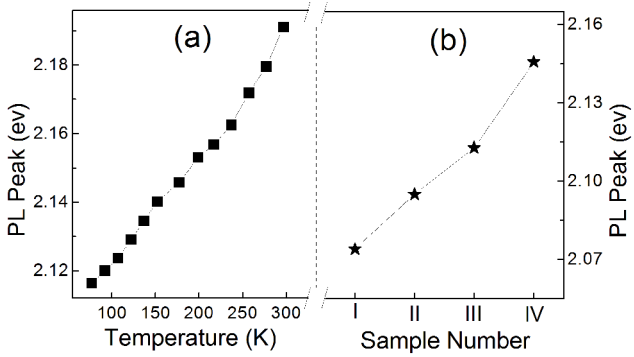

Figure 4: PL peaks of ZnSe:Mn/ZnSe NCs under elevating temperature (a) and Mn-doped NCs with strengthening binding symmetry (b).

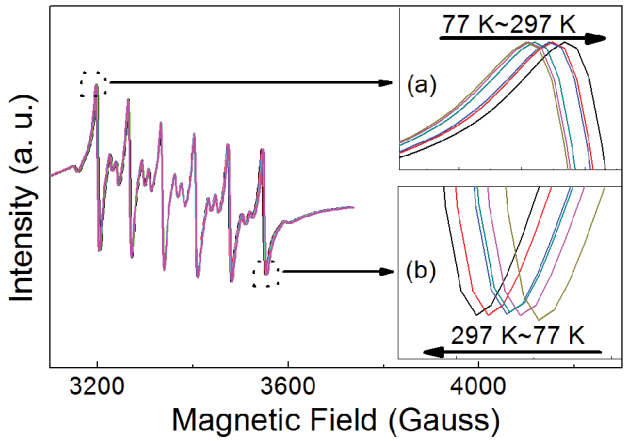

Figure 5: EPR spectra of the ZnSe:Mn/ZnSe NCs under different temperature (77, 112, 157, 192, 257, and 297 K). Insert (a) and (b) reveal the details of the EPR spectra around 3200 Gauss and 3550 Gauss, respectively. The inserts show the narrowing of the spectrum with increasing temperature.

into QDs successfully and no phase transformation was resulted from the doping. The ZnSe and ZnS patterns in Figure 2 demonstrate that sample II, III and IV have ZnS shells. The shift of (1 1 1) peak is due to the oppression of ZnS shell.

Typical PL spectra of ZnSe:Mn/ZnSe NCs under different temperature are shown in Figure 3. All the peaks are around 585 nm due to the transition from $^4T_1$ to $^6A_1$ [7,13,14]. The PL peaks of ZnSe:Mn/ZnSe NCs under different temperature and NCs with different binding symmetry are shown in Figure 4. The PL peak of ZnSe:Mn/ZnSe NCs shift to higher energy under elevating temperature (Figure 4a). This temperature-dependent trend demonstrates that increasing temperature results in smaller splitting of the $^6A_1$ state of Mn^{2+} ions in ZnSe:Mn/ZnSe NCs. Figure 4b shows the structure-dependent PL peak of the four samples. Except the PL shift resulted from the pressure of shell in core/shell NCs [17], the PL peak of NCs has a blue shift with decreasing binding symmetry. This also demonstrates smaller splitting of the $^6A_1$ state Mn^{2+} ions. Stronger crystal field results in bigger splitting of $^6A_1$ state of Mn^{2+}, which brings about red shift of the luminescence [23]. In this work, the PL peak shifts reflected by temperature-dependent and structure-dependent properties demonstrate that the strength of crystal field decreased.

Some previous reports have demonstrated the covalency between Mn^{2+} ions and the anions around them by the EPR spectra, which showed that increasing A value or/and decreasing g value correspond to weakening covalency [8,21,22,24]. Mn^{2+} ions have been doped into the NCs, which is indicated by the well-resolved hyperfine structure in Figure 5. No Mn-Mn pairs formed during the synthesis because there are no broad background lines in the spectra under different temperature [25]. Additional weak transitions between the six hyperfine lines due to spin forbidden transition are also observed. From the two inserts in Figure 5, the horizontal narrowing of the spectra was demonstrated with increasing temperature. It means that A becomes smaller in higher temperature. From Figure 6, decreasing A value can be observed both in ZnSe:Mn/ZnSe NCs under elevating temperature and NCs with more symmetrical binding structure. Meanwhile, all the values of A are 66.5~69.5, which indicates no Mn^{2+} ions are at the surface of NCs [19]. This agrees with the synthesis strategy and ensures that this work is based on the Mn^{2+} ions at the interface of the core/shell NCs. Figure 7 shows the g values of EPR spectra. In ZnSe:Mn/ZnSe NCs under elevating temperature and NCs with more symmetrical binding structure, g values become bigger. According to references [8,21,22,24] elevating temperature can resulted in stronger covalency in ZnSe:Mn/ZnSe NCs and more symmetrical binding structure also did this. The decreasing crystal field reflected by PL shift is interrelated to stronger covalency suggested by EPR spectra. This relationship between

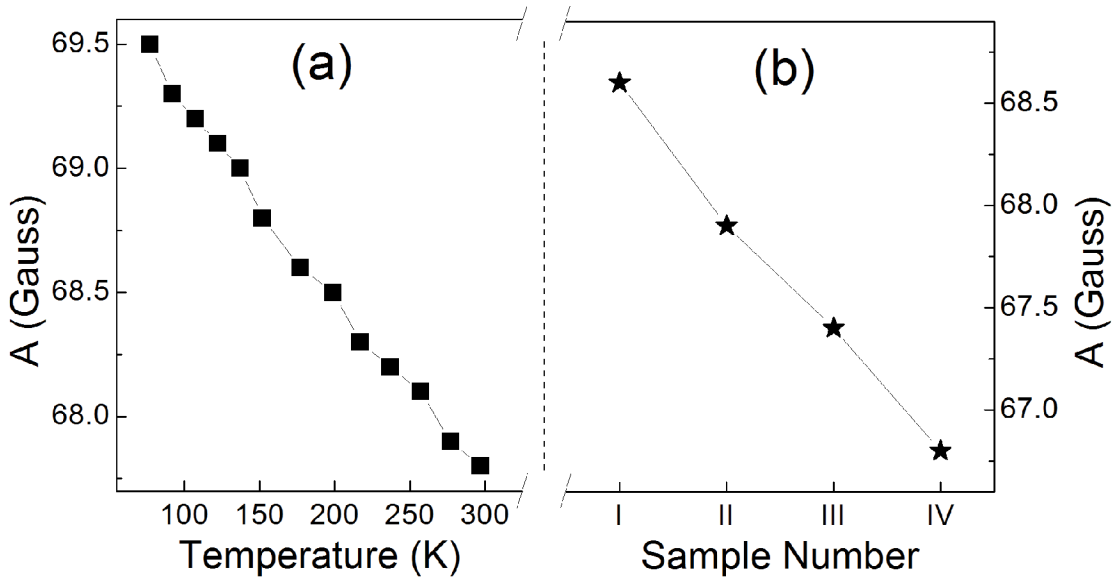

Figure 6: A (hyperfine splitting constant) values of ZnSe:Mn/ZnSe NCs under elevating temperature (a) and Mn-doped NCs with strengthening binding symmetry (b).

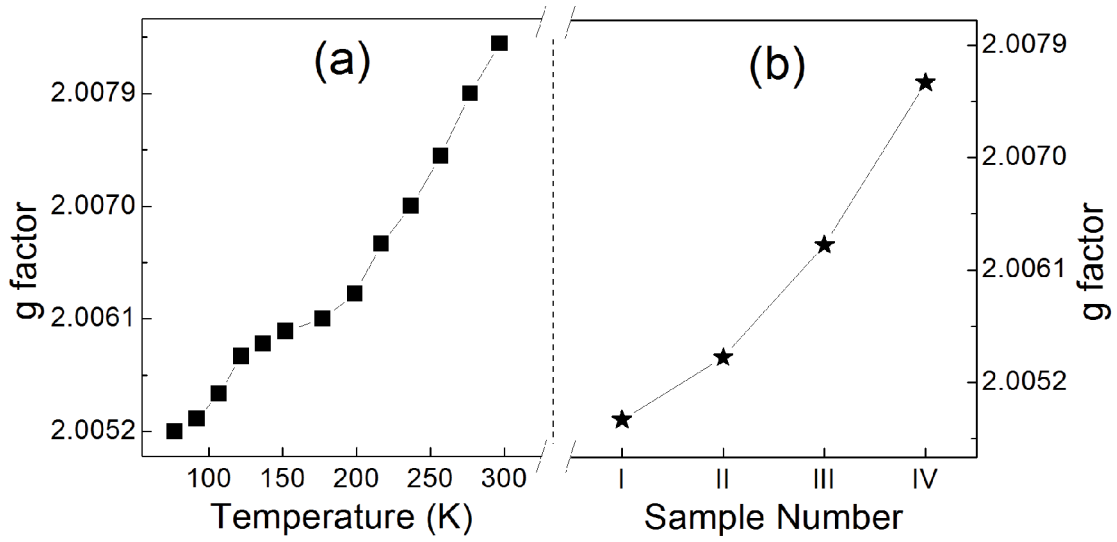

Figure 7: g values of ZnSe:Mn/ZnSe under elevating temperature (a) and Mn-doped NCs with strengthening binding symmetry (b).

crystal field and covalency is demonstrated by temperature-dependent and structure-dependent properties of Mn-doped NCs. This relationship can be interpreted as: the crystal theory is based on the ionic electrostatic field, so stronger covalency (weaker ionicity) weakens the crystal field.

Conclusion

In summary, PL and magnetic properties of NCs with different binding symmetry and ZnSe:Mn/ZnSe NCs under different temperature were discussed. Mn^{2+} ions were at the interface of the cubic core/shell NCs. Increasing crystal field and weakening covalency was associated through PL peaks and g/A values of the EPR spectra. Both temperature-dependent and structure-dependent results clarified this relationship.

References

1. AP Alivisatos (1996) Semiconductor clusters, nanocrystals, and quantum dots. Science 271: 933-937.
2. SA Empedocles, MG Bawendi (1997) Qutum-confined Stark effect in single CdSe nanocrystallite quantum dots. Science 278: 2114-2117.
3. CJ Wang, M Shim, P Guyot-Sionnest (2001) Electrochromic nanocrystal quantum dots. Science 291: 2390-2392.
4. RN Bhargava (1997) The role of impurity in doped nanocrystals. Journal of Luminescence 72: 46-48.

Citation: Yang B (2017) The Photoluminescent and Magnetic Properties of Mn^{2+} Ions at the Interface of Core/Shell Mn-Doped Nanocrystals. Int J Nanoparticles Nanotech 3:009

5. SC Erwin, LJ Zu, MI Haftel, AL Efros, TA Kennedy, et al. (2005) Doping semiconductor nanocrystals. Nature 436: 91-94.
6. DJ Norris, AL Efros, SC Erwin (2008) Doped nanocrystals. Science 319: 1776-1779.
7. N Pradhan, DM Battaglia, Y Liu, XG Peng (2007) Effecient, stable, small, and water-soluble doped ZnSe nanocrystal emitters as non-cadmium biomedical labels. Nano Letter 7: 312-317.
8. BP Yang, XC Shen, HC Zhang, YP Cui, JY Zhang (2013) Luminescent and magnetic properties in semiconductor nanocrystals with radial-position-controlled Mn^{2+} doping. J Phys Chem C 117: 15829-15834.
9. BP Yang, JY Zhang, YP Cui, K Wang (2011) White light-emitting diode coated with ZnSe:Mn/ZnSe nanocrystal films enveloped by SiO_2. Applied Optics 50: 137-141.
10. MR Kim, DL Ma (2015) Quantum-dot-based solar cells: recent advances, strategies, and challenges. J Phys Chem Lett 6: 85-99.
11. T Norman, D Magana, T Wilson, C Burns, JZ Zhang, et al. (2003) Optical and surface structural properties of Mn^{2+}-doped ZnSe nanoparticles. J Phys Chem B 107: 6309-6317.
12. LJ Zu, AW Wills, TA Kennedy, ER Glaser, DJ Norris (2010) Effect of different manganese precursors on the doping efficiency in ZnSe nanocrystals. J Phys Chem C 114: 21969-21975.
13. RN Bhargava, D Gallagher, X Hong, A Nurmikko (1994) Optical properties of manfanese-doped nanocrystals of ZnS. Phys Rev Lett 72: 416-419.
14. J Xue, Y Ye, F Medina, L Martinez, SA Lopez-Rivera, et al. (1998) Temperature evolution of the 2.1 eV band in the $Zn_{1-x}Mn_xSe$ system for low concentration. Journal of Luminescence 78: 173-178.
15. N Pradhan, D Goorskey, J Thessing, XG Peng (2005) An alternative of CdSe nanocrystal emitters: pure and stable impurity emissions in ZnSe nanocrystals. J Am Chem Soc 127: 17586-17587.
16. A Aboulaich, M Geszke, L Balan, J Ghanbaja, G Medjahdi, et al. (2010) Sulfur-metal orbital hybridization in sulfur-bearing compounds studied by X-ray emission spectroscopy. Inorg Chem 49: 10940.
17. S Ithurria, P Guyot-Sionnest, B Mahler, B Dubertret (2007) Mn^{2+} as a radial pressure gauge in colloidal core/shell nanocrystals. Phys Rev Lett 99: 265501.
18. D Zhu, Y Chen, L Jiang, J Geng, J Zhang, et al. (2011) Manganese-doped ZnSe quantum dots as a probe for time-resolved fluorescence detection of 5-fluorouracil. Anal Chem 83: 9076-9081.
19. BP Yang, XC Shen, HC Zhang, YP Cui, JY Zhang (2014) Temperature-dependent photoluminescence of Mn-doped ZnSe nanocrystals. Sci Adv Mater 6: 623-626.
20. S Bhattacharayya, I Perelshtein, O Moshe, DH Rich, A Gedanken (2008) One-step solvent-free synthesis and characterization ofZn1-xMnxSe@C nanorods and nanowires. Adv Funct Mater 18: 1641.
21. WW Zheng, ZX Wang, J Wright, B Goundie, NS Dalal, et al. (2011) Probing the local site environments in Mn:CdSe quantum dots. J Phys Chem C 115: 23305-23314.
22. YA Yang, O Chen, A Angerhofer, YC Cao (2008) On doping CdS/ZnS core/shell nanocrystals with Mn. J Am Chem Soc 130: 15649-15661.
23. W Park, TC Jones, W Tong, S Schön, M Chaichimansour, et al. (1998) Luminescence decay kinetics in homogeneously and delta-doped ZnS:Mn. J App Phys 84: 6852.
24. JY Liu, CX Liu, YG Zheng, D Li, W Xu, et al. (1999) Three types of site of Mn^{2+} in ZnS: Mn^{2+} nanocrystal/Pyrex glass composites. J Phys: Condens Matter 11.
25. TH Ji, WB Jian, JY Fang (2003) The first synthesis of $Pb_{1-x}Mn_xSe$ nanocrystals. J Am Chem Soc 125: 8448-8449.

Citation: Yang B (2017) The Photoluminescent and Magnetic Properties of Mn^{2+} Ions at the Interface of Core/Shell Mn-Doped Nanocrystals. Int J Nanoparticles Nanotech 3:009